

Spin and electronic correlations in gated graphene quantum rings

P. Potasz,^{1,2} A. D. Güçlü,¹ and P. Hawrylak¹

¹*Institute for Microstructural Sciences, National Research Council of Canada, Ottawa, Canada*

²*Institute of Physics, Wrocław University of Technology, Wrocław, Poland*

(Dated: September 13, 2018)

We present a theory of graphene quantum rings designed to produce degenerate shells of single particle states close to the Fermi level. We show that populating these shells with carriers using a gate leads to correlated ground states with finite total electronic spin. Using a combination of tight-binding and configuration interaction methods we predict ground state and total spin of the system as a function of the filling of the shell. We show that for smaller quantum rings, the spin polarization of the ground state at half filling depends strongly on the size of the system, but reaches a maximum value after reaching a critical size.

I. INTRODUCTION

There is currently significant interest in developing understanding of electronic properties [1–4, 7, 8] and applications [5–7] of graphene. Starting with graphene as a zero gap non-magnetic material, reducing the lateral size and controlling the shape and character of the edges opens the possibility of controlling the energy spectrum and hence electronic and magnetic properties of graphene nanostructures [10–14]. In particular, the zigzag edges are responsible for degenerate energy shells at the Fermi level [13, 15–19, 22], and associated finite spin polarization as a result of electron-electron exchange interactions [15–23]. However, the coupling of spin polarized zigzag edges was shown to be anti-ferromagnetic in graphene nanoribbons [15] with no net spin polarization. In contrast, in triangular graphene quantum dots spin polarized edges were shown to couple ferromagnetically leading to a finite magnetic moment [19–21, 23]. The purpose of this work is to answer the question whether it is possible to use graphene nanoribbons to build graphene nanostructures with finite magnetic moment. We show here that by designing a hexagonal ring from six ribbons we obtain a quantum system with degenerate shells in the energy spectrum. By filling these shells with additional electrons using metallic gate we obtain maximally spin polarized ground state for the half filling of the degenerate shell.

Semiconductor quantum rings have been investigated by a number of groups [24–27]. The ring geometry allows to observe quantum phenomena, e.g. persistent current and quantum interference effects [28], in particular Aharonov-Bohm (AB) oscillations [24]. The AB oscillations manifest themselves as periodic oscillations in the energy spectrum of the electronic system as a function of the number of flux quanta entering the ring [25]. The AB effect for a single electron in single lithographically defined semiconductor quantum ring [26], hole in a type-II semiconductor dot [27] and exciton [29, 30] in a finite ring, was demonstrated.

The Aharonov-Bohm conductance oscillations were

also recently observed in a graphene ring [31, 32]. The electronic properties of a single Dirac Fermion in graphene quantum rings were studied using effective mass [33, 34] and tight-binding methods [33, 35, 36]. Valley degeneracy in graphene was shown to be lifted by the magnetic field [33, 35] since the magnetic field has the opposite sign in the two valleys.

In this work we combine the tight binding method with the configuration method to determine the electronic and spin properties of graphene quantum rings with zig-zag edges as a function of the number of additional electrons controlled by the gate. We analyze the energy spectrum of quantum rings as a function of the width of the ring and its size. We find degenerate electronic shells near Fermi energy for the thinnest structures. We use configuration interaction method to treat exactly interaction of additional electrons in the degenerate shell as a function of shell filling. We determine the dependence of the spin polarization of the ground state as a function of the filling of the degenerate shell and the size of the structure. We show that by changing the size of the structures we control the splitting between levels in a degenerate shell which in turn significantly influences magnetic properties of the ground state. The stabilization of the spin phase diagram at a critical size of the ring is observed.

This paper is organized as follows. In Section II, we introduce both the tight-binding (TB) model for single particle levels and configuration interaction method for electron-electron interaction. In Section III, we show the method for constructing hexagonal ring structures with different width and length. Next, in section IV we present discussion of single particle energy spectra and explain the origin of the shell structure. In section V we analyze the effect of electron-electron interactions and spin properties of electrons in degenerate shells as a function of shell filling. Finally, in section VI we summarize obtained results.

II. MODEL AND METHOD

The single particle energy spectrum of Π_z electrons in graphene quantum rings can be obtained using the tight-binding Hamiltonian [37]. The tight-binding model was successfully applied to carbon materials such as graphite, graphene, nanoribbons, nanotubes, fullerenes, and graphene quantum dots [13, 14, 16–19, 37]. The Hamiltonian in the nearest neighbors approximation can be written as

$$H = t \sum_{\langle i,j \rangle, \sigma} c_{i\sigma}^\dagger c_{j\sigma}, \quad (1)$$

where t is the hopping integral, $c_{i\sigma}^\dagger$ and $c_{i\sigma}$ are creation and annihilation operators of electron on Π_z orbital on site i with spin $\sigma = \uparrow, \downarrow$ respectively, and $\langle i, j \rangle$ indicate summation over nearest-neighbours. Diagonalization of the tight-binding Hamiltonian generates single particle energies ϵ_s and single particle orbitals $|s, \sigma\rangle$.

In order to include electron-electron interactions the many-body Hamiltonian H_{MB} is written as

$$H_{MB} = \sum_{s, \sigma} \epsilon_s a_{s\sigma}^\dagger a_{s\sigma} + \frac{1}{2} \sum_{\substack{s,p,d,f, \\ \sigma, \sigma'}} \langle sp | \tilde{V} | df \rangle a_{s\sigma}^\dagger a_{p\sigma'}^\dagger a_{d\sigma'} a_{f\sigma}, \quad (2)$$

where the first term describes single particle energies obtained from the tight binding Hamiltonian given by Eq. (1) and the second term describes interactions between particles occupying these single particle states. By using Slater π_z orbitals [38] we calculated two-body Coulomb matrix elements $\langle ij | V | kl \rangle$, where i, j, k, l are the site indices. In numerical calculations, on-site and all scattering and exchange terms up to next nearest neighbor's are included. Few largest Coulomb matrix elements are given in the Appendix. We use $t = -2.5\text{eV}$ for the hopping integral, and the effective dielectric constant is set to $\kappa = 6$.

III. CONSTRUCTION OF GRAPHENE RINGS

In this section we show the method for constructing a mesoscopic ring from six graphene nanoribbons. Such a choice of building blocks helps us to understand single particle spectrum of the ring. In Fig. 1 we show two sets of six graphene ribbons arranged in a hexagonal ring. Each ribbon consists of two types of atoms from the unit cell of honeycomb lattice, indicated by red (light grey) and blue (dark grey) circles in Fig. 1. On the left side, thinnest possible ribbons with one benzene ring width are shown, denoted as $W = 1$. Each of them consists of 16 atoms (the length $L = 4$, is measured by the number of one type of atoms in the upper row), so the final ring

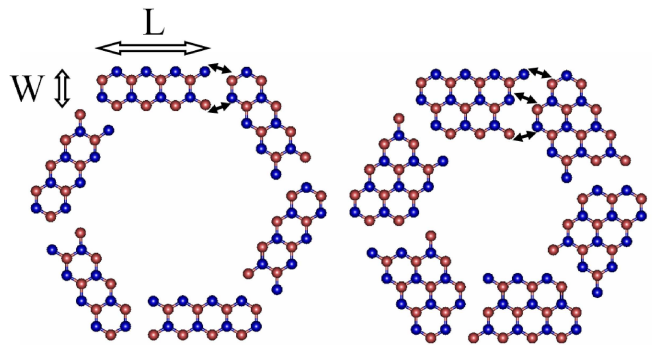


FIG. 1. (Color online) The method of construction of ring structures from smaller ribbon-like units. On the left, there are six thinnest possible ribbons (one benzene ring thick, what we note as $W = 1$) arranged in a hexagonal ring structure. The length of each ribbon is given by $L = 4$, the number of one type of atoms in one row. Each ribbon consists of 16 atoms which gives a total of 96 atoms in a ring. On the right, there are six ribbons with width $W = 2$ (two benzene ring thick). Each of them consists of 21 atoms giving a total of 126 atoms in a ring. We create a thicker ring with similar length ($L = 4$) but smaller antidot inside.

is built of 96 atoms. Small black arrows indicate bonds (and hopping integrals between nearest neighbors in a tight-binding model) between neighboring ribbons (two arrows in the case of thinnest structures). The number of such connecting atoms increases with increasing width as seen on the right hand side of Fig. 1. The thicker ribbon ($W = 2$) has identical length to the one from the left side ($L = 4$). In this case there are three connecting atoms (three small black arrows indicate three bonds). The final ring is built of 126 atoms. By connecting neighboring ribbons with different lengths and widths we create rings with different single particle spectra.

IV. SINGLE PARTICLE SPECTRA

In Fig. 2 we show the single-particle energy levels near Fermi level obtained by diagonalizing tight-binding Hamiltonian, Eq. (1), for rings with a given length ($L = 8$) and different widths. The thinnest ring ($W = 1$) consists of 192 atoms. For this structure we observe nearly degenerate shells of energy levels separated by gaps. Each shell consists of six levels: two single and two doubly degenerate states. First shell over the Fermi level is almost completely degenerate while in the second one the degeneracy is slightly removed. We note that for rings with different lengths, the gap between first and second shell is always larger than the gap at the Fermi level. With increasing width of the ring, the spectrum changes completely. For the rings with width $W = 2$ (270 atoms), $W = 3$ (336 atoms) and $W = 5$ (432 atoms) shells are

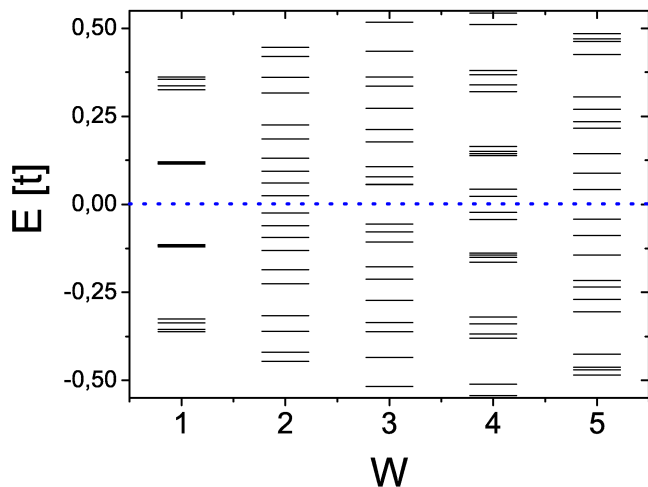


FIG. 2. (Color online) Single particle spectrum near Fermi level for ring structures with $L = 8$ and different widths. The shell structure is clearly observed only for the thinnest ring ($W = 1$). Dotted blue (grey) line indicate the location of Fermi energy.

not visible. For $W = 4$ (390 atoms) we observe appearance of shells separated by gaps further from Fermi level but the splitting between levels in these shells is much stronger in comparison to the thinnest ring. We note that for $W \geq 2$, although we do not observe a clear pattern of shells around the Fermi level, single shells of six levels separated by gaps from the rest of the spectrum appear far away from the Fermi energy in some cases.

In order to have a better understanding of the structure of the tight-binding spectra, in Fig. 3 we show the evolution of single particle energies from six independent ribbons to a ring as the hopping between the ribbons is increased. To achieve this, first we diagonalize tight-binding Hamiltonian matrix for a single ribbon. We then take six such ribbons and create Hamiltonian matrix in the basis of the eigenvectors of six ribbons. Here, the matrix has diagonal form. All energy levels are at least six fold degenerate. Next, using the six ribbons basis, we write hopping integrals corresponding to connecting atoms between neighboring ribbons (indicated by small black arrows in Fig. 1). By slowly turning on the hopping integrals and diagonalizing the Hamiltonian at every step, we can observe the evolution of the spectrum from single particle states of six independent ribbons to a ring.

The hopping integrals between connecting atoms of neighboring ribbons are indicated by t' in Fig. 3. For the thinnest ring (Fig. 3(a)), each ribbon consists of 32 atoms. There are only two connecting atoms between neighboring ribbons, giving only two hopping integrals t' between each two ribbons in the nearest neighbors approximation. We see that their influence is very small and six fold degenerate states evolve into shells with a very small splitting between levels. We note that this

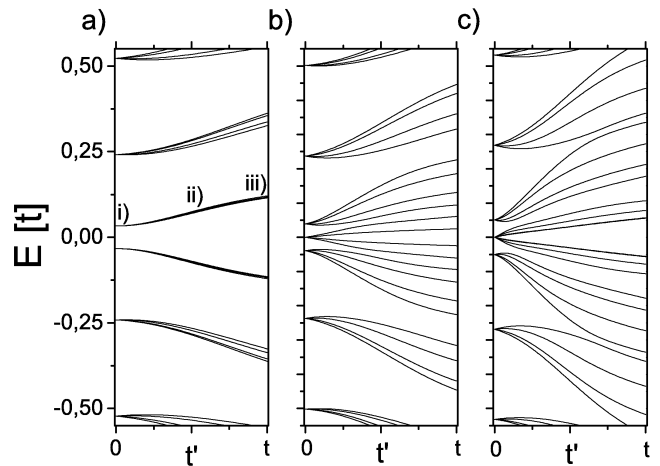


FIG. 3. (Color online) The evolution of the single particle spectrum from six independent ribbons with $L = 8$ to a hexagonal ring structure spectrum. t' indicate hopping integrals between neighboring ribbons. a) For the thinnest ring ($W = 1$) six fold degeneracy is slightly removed, preserving a shell structure. For thicker structures ((b) and (c), $W = 2$ and $W = 3$ respectively) the six fold degeneracy is strongly lifted and shell structure is not observed.

splitting is a bit stronger for higher energy levels but due to large gaps between consecutive levels of single ribbon the shell structure is still clearly observed. For the thicker structures (Fig. 3(b) and (c)) the evolution of the spectrum has a more complicated behavior. For a given ring each ribbon consists of different number of two types of atoms which give rise to zero energy edge-states [39]. With increasing width, the number of zero-energy states increases as well as the number of connecting atoms (and equally the number of t' hopping integrals). This causes a stronger splitting of levels for thicker rings in comparison to the thinnest one. Thus, the thicker ring's spectrum close to the Fermi level is due to the splitting of zero-energy states of independent ribbons. For $W = 2$ (one zero-energy state) and $W = 3$ (two zero-energy states), each ribbon consists of 45 and 56 atoms respectively, and the evolution of their spectrum is similar. The degeneracy is strongly lifted and no shell structure is observed.

In order to illuminate the influence of t' hopping integrals on the thinnest ring spectrum, in Fig. 4 we also show the electronic densities for the first shell over the Fermi level for three different values of t' (indicated in Fig. 3(a)). For $t' = 0$ there are six independent ribbons and first shell is perfectly six fold degenerate. The electronic charge density in each ribbon is larger on the two atoms with only one bond (see Fig.1) and gradually decreases along the length. For $t' = 0.5t$ the total energy of the shell increases and the degeneracy is slightly removed. Here, the highest peak of electronic charge density is moved towards the center of each ribbon in comparison to $t' = 0$ case. Increasing t' to t causes increasing

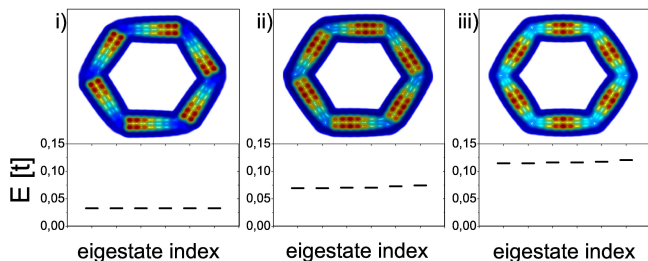


FIG. 4. (Color online) Energy levels and corresponding total electronic densities for the first six states over the Fermi level for the thinnest structure with $L = 8$ (192 atoms), for i) $t' = 0$, ii) $t' = 0.5t$, iii) $t' = t$. The three values of t' hopping integrals are indicated in Fig. 3(a).

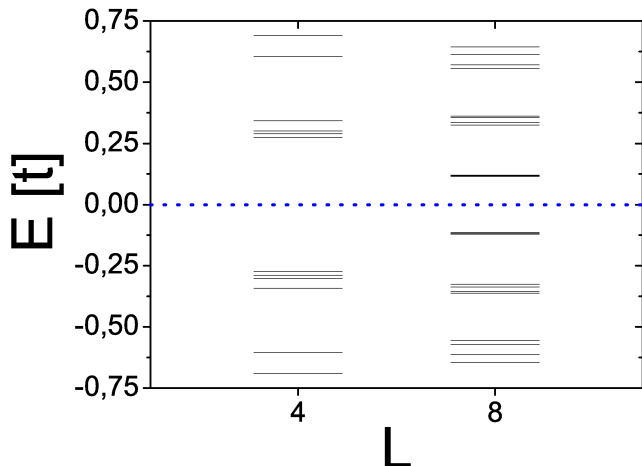


FIG. 5. (Color online) Single particle spectrum near Fermi level for the thinnest ring structures with length $L = 8$ and $L = 4$. The shell structure is clearly observed. The splitting between levels in the first shell is smaller for larger structure. Dotted blue (grey) line indicate the location of Fermi energy.

of the total energy of the shell and the highest peak of electronic charge density is now perfectly in the middle of each arm of the ring. Thus, both electronic charge density and energy of levels change slightly during the gradual transition of ribbons into a hexagonal ring structure.

We find degenerate shells near the Fermi energy only for the thinnest rings. In the rest of the paper, we will focus on the single and many particle properties of these structures as a function of their lengths. In Fig. 5 we show the low energy spectrum for two thinnest rings with different lengths. We clearly see shells with six levels. The splitting of levels from the first shell over the Fermi level is smaller for larger ring. For ring structure with $L = 4$ the difference between the highest and the lowest energy of levels forming the first shell is around $0.069t \approx 0.17$ eV. In comparison, for ring with $L = 8$ this value is around $0.006t \approx 0.015$ eV. Thus, we conclude

that for smaller rings single particle energies can play important role in the properties of many particle states while for the larger rings interactions are expected to be more important.

V. ELECTRONIC INTERACTIONS IN A DEGENERATE ELECTRONIC SHELL OF A GRAPHENE QUANTUM RING

In this section, we study ground and excited states as a function of the number of additional interacting electrons in degenerate shells of quantum rings with different size L . In our calculations we assume that all states below the Fermi level remain fully occupied. This is justified as long as there is a sufficiently large energy gap at the Fermi level. Next, we add extra electrons to the charge neutral system. In a first approximation we neglect scatterings from/to the states below Fermi energy. Moreover, because of the large energy gap between first and second shell we can neglect scatterings to the higher energy states. This allows us to treat first shell of the thinnest ring as an independent system which significantly reduces the dimension of the Hilbert space. All the shells in the studied structures consist of six levels. For a given number of extra electrons we create a basis of all possible configurations of electrons distributed within these states. Since the total spin of the system is conserved, we diagonalize the many-body Hamiltonian in subspaces with total projection of spin onto z-axis S_z . The largest dimension of the Hilbert space is for the half filling (6 electrons) and $S_z = 0$ for which there are 400 configurations.

First, we study the magnetic properties of the half filled shell. Figure 6 shows the low energy spectra for the different total spin S of half filled first shell over the Fermi energy for two thinnest rings with a) $L = 4$ (96 atoms) and b) $L = 8$ (192 atoms). For smaller ring the ground state has total spin $S = 1$ with a very small gap to the first excited state with $S = 0$ [40]. The lowest states with larger total spin have higher energies. For 192 atoms ring the total spin of the ground state is maximal ($S = 3$). The lowest levels with different total spin have slightly higher energies. This can be understood in a following way. The splitting between levels is large for smaller structures, which is seen in Fig. 5. For ring with $L = 4$ (96 atoms) this value (0.17 eV) is comparable with electronic interaction terms, e. g. 0.34 eV for two electrons occupying the lowest state. For ring with $L = 8$ (192 atoms) the electron-electron interaction terms are around 0.23 eV (for interaction between two particles on the first state), which is much larger in comparison with single particle energy difference (0.015 eV). From this, we clearly see that for ring with $L = 4$ it is energetically favorable to occupy low energy states by electrons with opposite spins. For ring with $L = 8$ all states have simi-

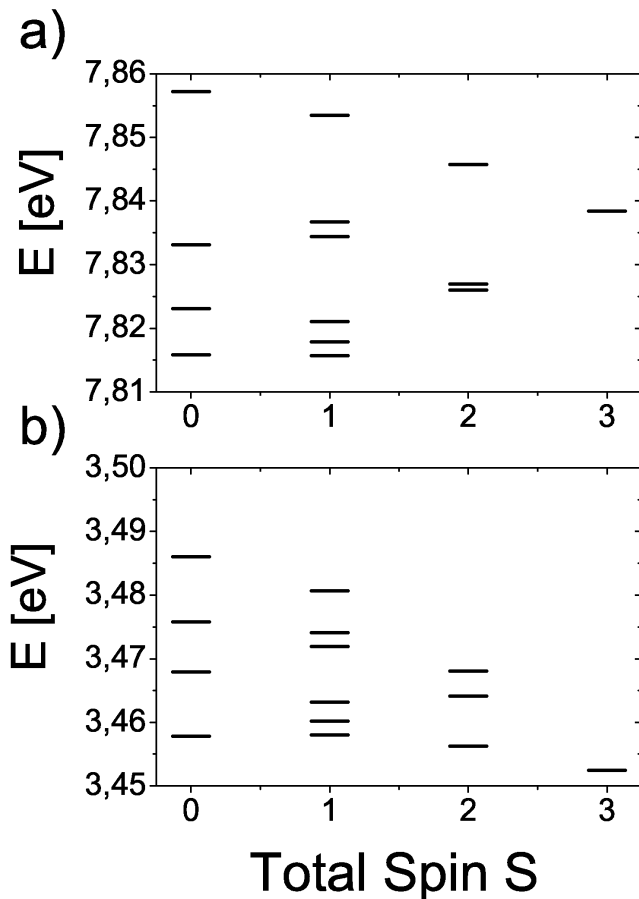


FIG. 6. (Color online) The low energy spectra for the different total spin S of half filled first shell over the Fermi energy for two thinnest rings with (a) $L = 4$ (96 atoms) and (b) $L = 8$ (192 atoms).

lar energies and due to exchange interactions the lowest energy state is maximally spin polarized.

The behavior of magnetic properties of the ground state for half filled shell as a function of size is shown in Fig. 7. In this case, ground state properties can be explained as a result of the competition between occupation of levels with smallest single particle energies which favors opposite spin configurations, and parallel spin configurations for which exchange interactions are maximized. For rings with $L \geq 5$ the ground state is maximally spin polarized. Here, the splitting between levels is relatively small and the ground state is determined by electronic interactions. Moreover, this splitting decreases with increasing size and this is seen in the spin gap behavior (Fig. 7). The largest spin gap is observed for ring with $L = 6$ and decreases with increasing L . For small rings the situation is more complicated. Here, the contributions from single particle energies and interactions are comparable. As a consequence, we observe ground states with alternating total spin $S = 1$ and $S = 0$. For sufficiently large rings, $L > 5$, we observe sta-

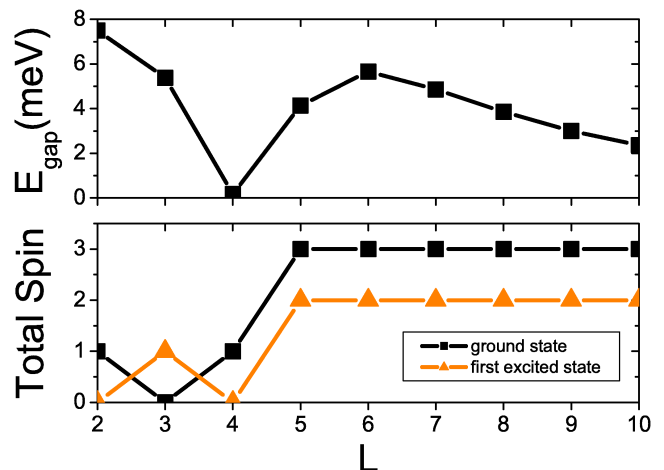


FIG. 7. (Color online) Lower: Total spin of the ground and first excited states for the half filling of the first shell in the thinnest ring structures with different sizes. Upper: Corresponding energy spin gap between ground and first excited states.

bilization of the spin phase diagram. This is connected to changes of the energy differences between levels in a shell - above a critical size these values are so small that they don't play a role anymore.

In Fig. 8 we show the phase diagram for a ring with $L = 8$ (192 atoms). Near the half filling the ground state is maximally spin polarized which is related to the dominant contribution from the short-ranged exchange interaction terms, and charge density is symmetrically distributed in the entire ring (see Fig. 4). Adding or removing electrons causes irregularities in the density distribution, and correlation effects start becoming important. This results in an alternating spin between maximal polarization (e.g. 3, 4, 9 extra electrons) and complete depolarization (e.g. 2, 8, 10 extra electrons) of the system.

VI. CONCLUSIONS

We presented here a theory of graphene quantum rings designed to produce degenerate shells of single particle states close to the Fermi level. By combining tight-binding and configuration interaction methods, we analyzed magnetic properties and electronic correlations in such structures as a function of size and number of added electrons. For the half filling of the degenerate shell in sufficiently large ring, maximal polarization of the ground state is predicted. Away from the half filling the correlation effects appear and the ground state total spin alternates between maximal polarization and complete depolarization.

Acknowledgment. The authors thank NRC-CNRS CRP, Canadian Institute for Advanced Research, Insti-

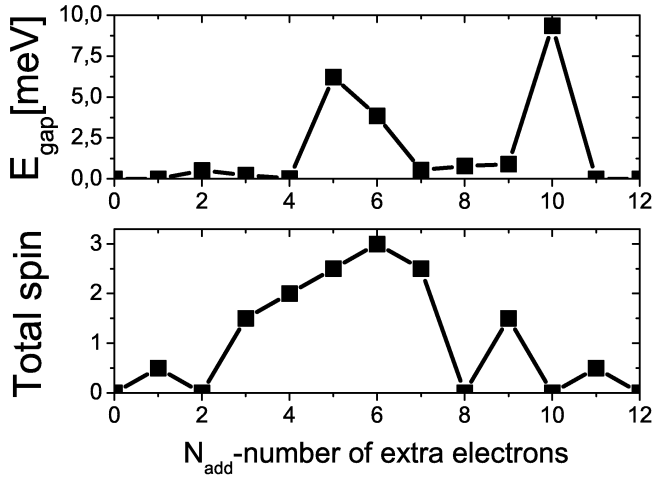


FIG. 8. (Color online) The spin phase diagram for electrons occupying first shell of the ring structure with $L = 8$ (192 atoms).

tute for Microstructural Sciences, QuantumWorks and Polish MNiSW, Grant No. N202-071-32/1513 for support.

APPENDIX A: CALCULATIONS OF COULOMB MATRIX ELEMENTS BETWEEN ELECTRONS ON SITES IN GRAPHENE HONEYCOMB LATTICE.

The Coulomb interaction term from eq. (2), we can write as

$$V = \frac{1}{2} \sum_{\substack{s,p,d,f, \\ \sigma,\sigma'}} \langle sp | V | df \rangle a_{s\sigma}^\dagger a_{p\sigma'}^\dagger a_{d\sigma'} a_{f\sigma}$$

$$= \frac{1}{2} \sum_{\substack{s,p,d,f, \\ \sigma,\sigma'}} \left[\sum_{\substack{i,j,k,l, \\ \sigma,\sigma'}} \langle ij | \tilde{V} | kl \rangle A_i^s A_j^p A_k^d A_l^f c_{i\sigma}^\dagger c_{j\sigma'}^\dagger c_{k\sigma'} c_{l\sigma} \right],$$

where we substitute $a_{s\sigma} = \sum_{i\sigma} A_i^s c_{i\sigma}$ and A_i^s are coefficients in transformation from one basis to another. Here the Coulomb matrix elements are defined as

$$\langle ij | \tilde{V} | kl \rangle = \frac{e^2}{4\pi\kappa} \int \int d\mathbf{r}_1 d\mathbf{r}_2 \psi_i^*(\mathbf{r}_1) \psi_j^*(\mathbf{r}_2) \times \frac{1}{|\mathbf{r}_2 - \mathbf{r}_1|} \psi_k(\mathbf{r}_2) \psi_l(\mathbf{r}_1)$$

where κ is an effective dielectric constant and $\psi_i(\mathbf{r}_1)$ is Slater π_z orbital on a site i of electron 1, given by a function

$$\psi(\mathbf{r}_1) = \left(\frac{\xi^5}{32\pi} \right)^{\frac{1}{2}} z \exp\left(\frac{-\xi \mathbf{r}_1}{2} \right),$$

with $\xi = 3.14$. Below we show selected Coulomb matrix elements for $\kappa = 1$. Numbers 1 and 2 and 3 indicate

$\langle ij \tilde{V} kl \rangle$	E [eV]
$\langle 11 \tilde{V} 11 \rangle$	16.522
$\langle 12 \tilde{V} 21 \rangle$	8.640
$\langle 13 \tilde{V} 31 \rangle$	5.333
$\langle 11 \tilde{V} 12 \rangle$	3.157
$\langle 12 \tilde{V} 31 \rangle$	1.735
$\langle 12 \tilde{V} 12 \rangle$	0.873
$\langle 11 \tilde{V} 22 \rangle$	0.873
$\langle 22 \tilde{V} 13 \rangle$	0.606

TABLE I. Selected coulomb matrix elements between electrons on sites in graphene honeycomb lattice.. Numbers 1, 2 and 3 indicate electron on-site, on nearest neighbor site and on next nearest neighbor site of hexagonal lattice, respectively.

electron on-site and on nearest neighbor site and on next nearest neighbor site of hexagonal lattice, respectively:

- [1] K. S. Novoselov, A. K. Geim, S. V. Morozov, D. Jiang, Y. Zhang, S. V. Dubonos, I. V. Grigorieva, and A. A. Firsov, *Science* **306**, 666 (2004).
- [2] K. S. Novoselov, A. K. Geim, S. V. Morozov, D. Jiang, M. I. Katsnelson, I. V. Grigorieva, S. V. Dubonos, and A. A. Firsov, *Nature* **438**, 197 (2005).
- [3] Y. B. Zhang, Y. W. Tan, H. L. Stormer, and P. Kim, *Nature* **438**, 201 (2005).
- [4] A. Rycerz, J. Tworzydło, and C. W. Beenakker, *Nature Phys.* **3**, 172 (2007).
- [5] T. Mueller, F. Xia, and P. Avouris, *Nature Photon.* **4**, 297 (2010).
- [6] F. Xia, T. Mueller, Y.-M. Lin, A. Valdes-Garcia, and P. Avouris, *Nature Nanotechnol.* **4**, 839 (2009).
- [7] A. K. Geim, K. S. Novoselov, *Nat. Mater.* **6**, 183 (2007).
- [8] A. H. C. Neto, F. Guinea, N. M. R. Peres, K. S. Novoselov, and A. K. Geim, *Rev. of Mod. Phys.* **81**, 109 (2009).
- [9] L. C. Campos, V. R. Manfrinato, J. D. Sanchez-Yamagishi, J. Kong, and P. Jarillo-Herrero, *Nano. Lett.* **9**, 2600 (2009).
- [10] H. P. Heiskanen, M. Manninen, and J. Akola, *New J. Phys.* **10**, 103015 (2008).
- [11] Z. Z. Zhang, K. Chang, and F. M. Peeters, *Phys. Rev. B* **77**, 235411 (2008).
- [12] D. A. Bahamon, A. L. C. Pereira, and P. A. Schultz, *Phys. Rev. B* **79**, 125414 (2009).
- [13] M. Ezawa, *Phys. Rev. B* **73**, 045432 (2006).
- [14] K. Nakada, M. Fujita, G. Dresselhaus, and M. S. Dresselhaus, *Phys. Rev. B* **54**, 17954 (1996).
- [15] Y. Son, M. L. Cohen, and S. G. Louie, *Nature* **444**, 347 (2006).
- [16] T. Yamamoto, T. Noguchi, and K. Watanabe, *Phys. Rev. B* **74**, 121409 (2006).
- [17] M. Ezawa, *Phys. Rev. B* **76**, 245415 (2007).
- [18] M. Ezawa, *Phys. Rev. B* **77**, 155411 (2008).
- [19] J. Fernandez-Rossier and J. J. Palacios, *Phys. Rev. Lett.* **99**, 177204 (2007).

- [20] A. D. Güçlü, P. Potasz, O. Voznyy, M. Korkusinski, and P. Hawrylak, *Phys. Rev. Lett.* **103**, 246805 (2009).
- [21] W. L. Wang, S. Meng, and E. Kaxiras, *Nano Letters* **8**, 241 (2008).
- [22] B. Wunsch, T. Stauber, F. Sols, and F. Guinea, *Phys. Rev. Lett.* **101**, 036803 (2008).
- [23] W. L. Wang, O. V. Yazyev, S. Meng, and E. Kaxiras, *Phys. Rev. Lett.* **102**, 157201 (2009).
- [24] Y. Aharonov, and D. Bohm, *Phys. Rev.* **115**, 485 (1959).
- [25] R. A. Webb, S. Washburn, C. P. Umbach, and R. B. Laibowitz, *Phys. Rev. Lett.* **54**, 2696 (1985).
- [26] M. Bayer, M. Korkusinski, P. Hawrylak, T. Gutbrod, M. Michel, and A. Forchel, *Phys. Rev. Lett.* **90**, 186801 (2003).
- [27] E. Ribeiro, A. O. Govorov, W. Carvalho, Jr., and G. Medeiros-Ribeiro, *Phys. Rev. Lett.* **92**, 126402 (2004).
- [28] M. Buttiker, Y. Imry, and R. Landauer, *Phys. Lett.* **96**, 365 (1983).
- [29] R. A. Romer, and M. E. Raikh, *Phys. Rev. B* **62**, 7045 (2000).
- [30] M. D. Teodoro, V. L. Campo, Jr., V. Lopez-Richard, E. Marega, Jr., G. E. Marques, Y. Galvao Gobato, F. Iikawa, M. J. S. P. Brasil, Z. Y. AbuWaar, V. G. Dorogan, Yu. I. Mazur, M. Benamara, and G. J. Salamo, *Phys. Rev. Lett.* **104**, 086401 (2010).
- [31] S. Russo, J. B. Oostinga D. Wehenkel H. B. Heersche S. S. Sobhani L. M. K. Vandersypen, and A. F. Morpugo, *Phys. Rev. B* **77**, 085413 (2008).
- [32] M. Huefner, F. Molitor A. Jacobsen A. Pioda C. Stampfer K. Ensslin, and T. Ihn, *Phys. Status Solidi (b)* **246**, 2756 (2009).
- [33] P. Recher, B. Trauzettel, A. Rycerz, Ya. M. Blanter, C. W. J. Beenakker, and A. F. Morpugo, *Phys. Rev. B* **76**, 235404 (2007).
- [34] D. S. L. Abergel, V. M. Apalkov, and T. Chakraborty, *Phys. Rev. B* **78**, 193405 (2008).
- [35] J. Wurm, M. Wimmer, H. U. Baranger, and K. Richter, *Semicond. Sci. Technol.* **25**, 034003 (2010).
- [36] P. H. Rivera, A. L. C. Pereira, and P. A. Schulz, *Phys. Rev. B* **79**, 205406 (2009).
- [37] P. R. Wallace, *Phys. Rev.* **71**, 622 (1947).
- [38] B. J. Ransil, *Rev. Mod. Phys.* **32**, 245 (1960).
- [39] E. H. Lieb, *Phys. Rev. Lett.* **62**, 1201 (1989).
- [40] P. Potasz, A. D. Güçlü, and P. Hawrylak, *Acta Phys. Pol. A* **116**, 832 (2009).